Title Page

Highly-Active and Contaminant-Tolerant Cathodes for Durable Solid Oxide Fuel Cells

Final Report

Reporting Period: 10/01/2017 – 03/31/2020

DOE Contract No.: DE-FE0031201

DOE Project Manager: Steven Markovich

Prepared by
Yucun Zhou, Yu Chen, Nicholas Kane, and Meilin Liu

Center for Innovative Fuel Cell and Battery Technologies
School of Materials Science and Engineering
Georgia Institute of Technology
Atlanta, GA 30332-0245

Report Issued: April 2020

DISCLAIMER

This report was prepared as an account of work sponsored by an agency of the United States Government. Neither the United States Government nor any agency thereof, nor any of their employees, makes any warranty, express of implied, or assumes any legal liability or responsibility for the accuracy, completeness, or usefulness of any information, apparatus, product, or process disclosed, or represents that its use would not infringe privately owned rights. Reference herein to any specific commercial product, process, or service by trade name, trademark, manufacturer, or otherwise does not necessarily constitute or imply its endorsement, recommendation, or favoring by the United States Government or any agency thereof. The views and opinions of authors expressed herein do not necessarily state or reflect those of the United States Government or any agency thereof.

ABSTRACT

The objective of this project is to investigate the fundamental degradation methods occurring in solid oxide fuel cell (SOFC) cathodes when exposed to chromium and carbon dioxide contamination and to rationally design alkaline earth-based catalysts to increase stability and tolerance to contaminate poisoning. With a mechanistic and fundamental understanding of the degradation methods, advanced catalytic surface modifications can be applied to reduce degradation. The specific technical objectives are: (1) To identify/develop new catalysts (alkaline-earth based-) that are compatible chemically with the state-of-the-art cathode materials at high temperatures required for fabrication and with contaminates commonly encountered under operating conditions; (2) To improve the infiltration process for optimal control of the thickness, composition, and uniformity of the catalyst coatings; (3) To evaluate the electro-catalytic activity toward ORR of the chemically-stable materials when exposed to different types of contaminants using electrical conductivity relaxation measurements on bar samples and performance evaluation of catalyst-infiltrated cathodes; (4) To unravel the contamination-tolerant mechanisms of the new catalyst coatings under realistic environmental conditions (with different types of contaminants) using powerful *in situ* and *in operando* characterization techniques performed on model cells with thin-film/pattern electrodes, as guided by modeling and simulation; (5) To establish scientific basis for rational design of new catalysts of high tolerance to contaminants; (6) To validate the long term stability of modified LSCF cathodes in commercially available cells/stacks under ROC.

Alkaline earth-based catalysts have been systematically explored and tested under various contamination conditions. $BaCoO_{3-\delta}$ (BCO) was shown to produce the best catalytic activity enhancement as well as stability in a variety of contaminating conditions, including CO_2 and chromium. The microstructural evolution was investigated with SEM, EDS, and Raman spectroscopy, showing the BCO catalyst prevents the formation of insulating $SrCrO_4$ by forming electrically conductive $BaCrO_4$. Electrochemical relaxation measurements determined the BCO catalyst coatings increased the surface diffusion coefficient but did not significantly affect the diffusion coefficient and determined an optimum surface modification layer of 100 nm. A novel $Ba_{0.9}Co_{0.7}Fe_{0.2}Nb_{0.1}O_x$ (BCFN) catalyst was also shown to have excellent stability in chromium containing atmospheres. A novel surface sol-gel (SSG) surface modification, which offers superior thickness and compositional control, was applied to SOFCs to produce BaO catalyst coatings. SSG BaO coatings were shown to produce conformal coatings on the electrode surface, greatly

increasing stability in chromium containing atmospheres. An atomic level mechanistic approach was applied to investigate the stability of $PrBa_{0.8}Ca_{0.2}Co_2O_{5+\delta}$ (PBCC) with respect to a variety of common contaminants, demonstrating thermodynamically its superior stability in CO_2 containing atmospheres. Finally, the best catalyst coatings demonstrated in this project, BCO and PBCC, were applied to full cells which demonstrated superior stability for over 300 hours in CO_2 and Cr atmospheres.

Contents

Title Page 1

DISCLAIMER 2

ABSTRACT 3

1. Introduction 6

2. Executive Summary 8

3. Results and Discussion 9

3.1 Determination of the Best Alkaline Earth Catalysts 9

3.2 Electrochemical Relaxation Analysis of Catalyst Coatings 15

3.3 Fundamental Investigation of Catalysts Coatings using Model Cells 17

3.4 Atomic-level understanding of contaminates-tolerance enhancement 23

3.5 Advanced Deposition of Catalyst Coatings using Surface Sol-gel 25

3.6 Demonstration of Catalyst Coatings on Full Cells 29

4. Conclusions 33

Acronyms 33

Publications 34

References 35

1. Introduction

The demand for clean, secure, and sustainable energy has stimulated great interest in fuel cells for efficient energy conversion. Among all types of fuel cells, solid oxide fuel cells (SOFCs) are the cleanest, most efficient chemical-to-electrical energy conversion systems. Another remarkable advantage of SOFCs is their excellent fuel flexibility, offering potential for direct utilization of hydrocarbon fuels, coal gas, biomass, and other renewable fuels.[1-4] SOFC technologies could provide an economic bridge between the fossil fuel and hydrogen-fuel economies because they can run on both fossil fuels and hydrogen.[5, 6] While small SOFC systems appear poised for commercialization in distributed generation, broad market penetration will require continuous innovation of materials and fabrication processes to prolong system lifetime and reduce cost. One technical opportunity is to enhance the durability of the cathode, which continues to contribute the greatest performance degradation and efficiency loss in the existing SOFCs.[7]

The causes of cathode degradation include (i) coarsening of the microstructure over time; (ii) decomposition of cathode materials; (iii) chemical reaction with electrolyte during fabrication; (iv) delamination from electrolyte; and (v) contaminant poisoning.[8] To date, however, the degradation rates of real SOFC stacks are still much greater than the target set by the DOE-SECA program for commercial applications: ~ 0.2% per 1,000 hours for a lifetime longer than 40,000 hours.[9] For example, an average degradation rate as high as 1.4% per 1,000 hours has been reported for a stack using an LSCF cathode operated at 750°C over 10,000 hours.[10] Poisoning effects of volatile contaminants represent a major stumbling block to the realization of a durable SOFC stack, including chromium (Cr) from typical Cr-containing interconnect materials, boron (B) from sealing glasses, and sulfur (S) from the air stream under SOFC operating conditions.[11] In reality, it is impossible to fully prevent the exposure of cathode materials to various contaminants (e.g., Cr, H_2O, and CO_2) from cell/stack components and from the air stream. It is thus crucial to obtain a fundamental understanding of the degradation of SOFC cathodes and implement an effective approach to minimize the degradation effect. One prominent cathode degradation process is Cr-poisoning, when a typical Cr-containing material is used as the interconnect or other part in SOFC stacks.[8] It is well accepted that, in an oxidizing atmosphere at high temperatures, volatile Cr species such as CrO_3 and $Cr(OH)_2O_2$ are generated over the Cr oxide scale intrinsic to these alloys. However, it is still unclear how these Cr-containing species interact with the cathode under realistic operating conditions and result in degradation of cathode

performance. The deposition of Cr species is believed to be mainly due to the electrochemical reduction of gaseous Cr species to solid Cr_2O_3, which may compete with the oxygen reduction reaction. Konysheva et al[12] explained that Cr-poisoning of cathodes has a *physical* origin: the poorly conductive phases (e.g., $SrCrO_4$) with low ORR activity block the transport of oxygen species to the triple-phase-boundaries (TPBs). However, Jiang et al[13-16] proposed that Cr deposition on SOFC cathode is a non-electrochemical process, kinetically limited by nucleation reactions between the gaseous Cr species and nucleation agents (e.g., Mn and Sr). In an LSM cathode, Cr deposition is controlled by a chemical dissociation, which is initiated by the nucleation reaction between the gaseous Cr species and manganese species (i.e. Mn^{2+}). The interaction between the Mn^{2+} ions and the gaseous CrO_3 species would lead to the formation of Cr–Mn–O_x nuclei. The formation of stable Cr–Mn–O_x nuclei, in turn, accelerates the crystallization and grain growth of Cr_2O_3 oxide and $(Cr,Mn)_3O_4$ spinel phases. Similarly, in an LSCF cathode, the nucleation agent is identified to be SrO segregated to the surface of LSCF cathode, which subsequently promotes the formation of a Cr-Sr-O_x phase that accelerates the crystallization and growth of $SrCrO_4$. The formation of $(Cr,Mn)_3O_4$ on LSM and $SrCrO_4$ on LSCF resulted in performance degradation. Consequently, they proposed that cathode materials, which are free of nucleation agents (such as Mn and Sr), would be more tolerant toward Cr deposition. A typical material, $La(Ni,Fe)O_{3-\delta}$ (LNF) was thus proposed and demonstrated to be tolerant toward Cr-poisoning in comparison to the LSM cathode in subsequent studies[17, 18]. However, Stodolny et al[19-21] recently found that LNF was not stable when exposed to Cr-containing alloys; Ni atoms occupying the B-site can be replaced by Cr to form a secondary phase with lower conductivity, even at a temperature as low as 600ºC. They attributed the inconsistency with other studies to the microstructure of the cathode and concluded that Cr-poisoning depends strongly on cathode microstructure and operating temperatures, signifying the importance of cathode microstructures or architectures.

In this project, an effective strategy toward enhancing the durability and performance of the cathode materials for accelerating the commercialization of SOFC technologies was developed. These alkaline earth-based catalyst surface modifications fabricated via solution infiltration have greatly increased stability and increase catalytic activity towards ORR.

2. Executive Summary

We have demonstrated the feasibility of enhancing the electro-catalytic activity and stability of a porous LSCF cathode by infiltration of a proper catalyst coating [22-24]. The main advantages of surface modification of electrodes through infiltration are threefold. ***First*,** it has minimum impact on the existing SOFC structure and fabrication process but is an effective approach to drastically enhancing the durability while improving the electro-catalytic activity at a low cost. ***Second***, it allows the utilization of a wide variety of active materials that may not be otherwise used in a conventional electrode fabrication process due to high reactivity with other components of the SOFC or high cost, since the infiltration process separates the formation temperature of the catalytic active phase from the high sintering temperature required to guarantee a good binding interface between electrolyte and electrode, and it requires much less material compared to the standard electrode fabrication process. ***Third***, it allows the use of nano-sized and/or nano-structured surfaces and interfaces. When carefully designed, nano-architectured cathodes can outperform the existing SOFC systems because of higher surface areas of catalytically active materials or larger number of active sites, thus exerting more "microstructural effects" on contaminant-poisoning tolerance as discussed earlier. Improved performance and stability have been demonstrated in our recent studies using thin-film coating of LSM[25], PSM and PSCM,[7, 24] SSC [26], LCC[27], and SDC[28] on LSCF surface. It is desirable to achieve excellent durability while maintaining high electro-catalytic activity of the state-of-the-art SOFC cathode materials by surface modification through infiltration – a simple and cost-effective process.

In this project, electrochemical performance of blank LSCF has been evaluated at 750 ºC in the presence of different contaminants. A degradation mechanism for LSCF cathodes under realistic operating conditions with different types of contaminants has been proposed and unraveled using *in-situ* and *ex-situ* measurements. The microstructural and compositional evolution of LSCF cathodes as well as the cathode/electrolyte interfaces under realistic operating conditions has been studied. A variety of alkaline earth-based catalysts have been studied and it was shown that $BaCoO_{3-\delta}$ (BCO) coatings offer superior catalytic improvement and stability. In addition, a novel $Ba_{0.9}Co_{0.7}Fe_{0.2}Nb_{0.1}O_x$ (BCFN) catalyst has been shown to have extreme stability in chromium containing atmospheres.

The significant findings can be briefly summarized as follows:

- Evaluated the effect of infiltration volume and firing temperature on the ORR activity of cathodes using symmetrical cells;
- Evaluated the electro-catalytic activity toward ORR of the bare- and alkaline earth-based catalyst modified LSCF in air with a variety of contaminates;
- Evaluated the effect of different Ba-based catalysts such as $BaMO_x$ (M=Co, Ce, Zr, Ni) on the ORR kinetics and durability of LSCF electrodes in air with CO_2 and Cr contaminants;
- Developed a robust method for the deposition of a thin-film catalyst layer on LSCF bar samples for reliable determination of the surface exchange coefficients and oxygen diffusivity using electrical conductivity relaxation (ECR) measurements;
- Measured the surface exchange coefficient (k) and chemical diffusion coefficient (D) of bare and coated LSCF and determined the optimal thicknesses of ORR catalysts coated on an LSCF backbone electrode using ECR measurements;
- Fabricated and characterized thin-film ORR catalyst coated LSCF model cells using Raman spectroscopy, providing vital insight into the catalytic activity of the surface modification
- Developed an atomic-level understanding of the mechanism for enhancing contaminate tolerance of electrode materials;
- Determined the mechanism for promotion of the oxygen reduction reaction (ORR) by application of BaO nanoparticles;
- Developed low-cost and applicable surface sol-gel deposition techniques for large cathodes (~1 inch diameter) and demonstrated the stability of BaO SSG coating under various contaminates;
- Demonstrated the performance of novel $Ba_{0.9}Co_{0.7}Fe_{0.2}Nb_{0.1}O_x$ (BCFN) solution infiltration coatings for the prevention of chromium contamination;

3. Results and Discussion

3.1 Determination of the Best Alkaline Earth Catalysts

The early phases of this project focused on screening of different alkaline earth catalysts to determine the most catalytically active and stable catalyst for surface modification. Initial screening of many different catalysts was performed via solution infiltration.

The solution infiltration coatings in this project were achieved with a simple process, shown in Figure 1. To form the baseline cell, the $Sm_{0.2}Ce_{0.8}O_{2-\delta}$ (SDC) electrolyte pellet was pressed and sintered. Then, $La_{0.6}Sr_{04}Co_{0.2}Fe_{0.8}O_{3-\delta}$ (LSCF) tapes, fabricated via tape casting, were bonded to the pellet using an SDC slurry and the cell was sintered. To perform the solution infiltration, nitrate solutions containing the desired catalyst metal cations were dropped onto the porous electrode, followed by firing. The initial experiments focused on different catalyst materials, infiltration volumes (from 5-15 µL), and firing temperatures (from 800-1000 °C).

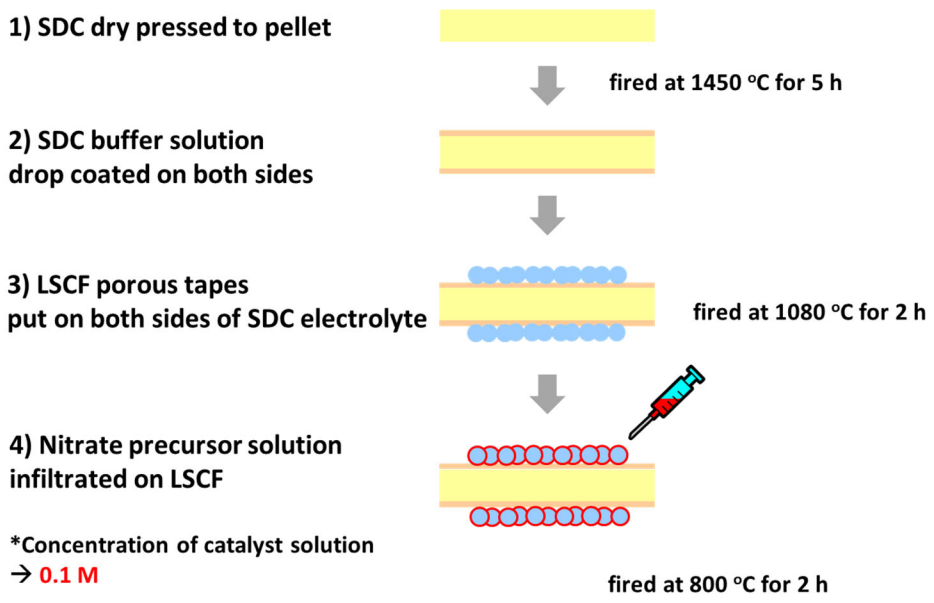

Figure 1. Schmatic of the typical solution infilration process.

Simple alkaline earth oxides, such as BaO, SrO, and CaO, were shown to decrease polarization resistance and increase stability of the LSCF electrode, while MgO is shown to have a detrimental effect on the performance.

The best catalytic activity and stability was achieved with bimetallic oxides, including $CaCoO_{3-\delta}$, $SrCoO_{3-\delta}$ (SCO), and $BaCoO_{3-\delta}$ (BCO), with BCO achieving the best performance and SCO slightly below that of BCO. Figure 2 shows the morphology and electrochemical performance of the BCO catalyst cells. Obvious BCO particles can be seen on the surface of the LSCF. Impedance spectroscopy analysis displays great improvement in stability versus the bare cell. From Figure 2d, it can be seen that the BCO coating reduced the initial polarization resistance, attributed to an increase in catalytic activity towards ORR, as well as greatly increased the stability

of the polarization resistance over time, attributed to reduced degradation of the cell. In addition, XRD investigations revealed no obvious reaction between the coating material and the LSCF backbone.

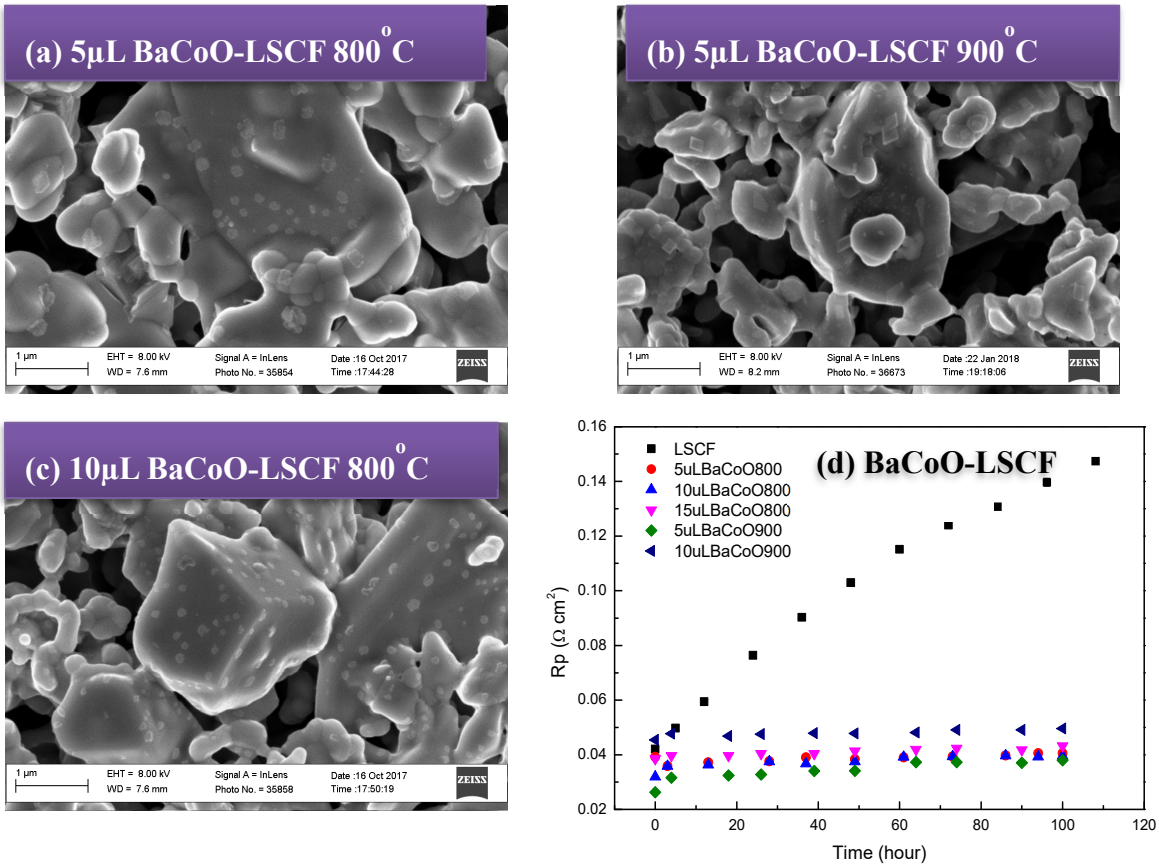

Figure 2. The morphology of LSCF cathode coated with BaCoOx catalyst, fired at (a) 800 °C, (b) 900 °C and (c) 800 °C for 2 hours, after testing in ambient air at 750 °C for 100 hours. (d) The short-term Rp testing (~100h) of LSCF cathode coated with BaCoOx catalyst with different firing temperatures.

The initial screening also produced a few significant tends observed with the catalysts examined. Increasing the firing temperature after infiltration increases the particle size of the catalyst particles on the surface. Additionally, increasing the infiltration volume improves stability, but can also increase polarization resistance.

After initial screening, the better performing catalysts were tested for stability against different contamination sources, including 3% H_2O, Cr+3% H_2O, CO_2 and SO_2. The catalysts showed improved stability to all contamination sources compared to bare LSCF. Figure 3 shows the R_p as a function of time in chromium contaminated air, displaying both initial catalytic improvements and increases in stability. Figure 4 shows EDS analysis of the cells after testing in

chromium, displaying a great reduction in the chromium detected for the BCO coated cell, which is supported by the improved electrochemical performance. Thus BCO has proved to be an effective catalyst to improve the performance in chromium containing atmospheres.

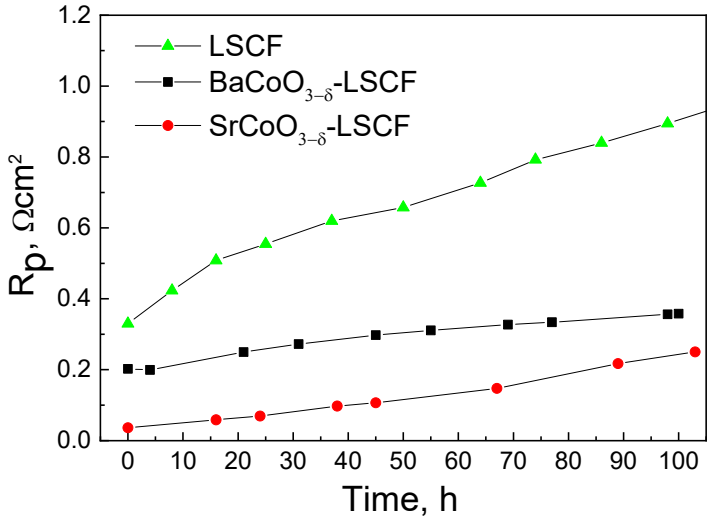

Figure 3. Long-term testing of blank LSCF, BCO and SCO catalyst coated on the LSCF cathode in symmetric cells. The amount of catalyst is 5μL 0.1M solution, which was fired at 900 °C for 2 hours. The testing condition is under Cr + 3 vol% H_2O at 750 °C for 100 hours.

Element	Wt.%	Atomic %
La	9.63	2.07
Sr	26.89	9.18
Fe	5.14	2.75
O	37.21	69.55
Cr	**12.75**	**7.33**
Si	4.07	4.34
Al	4.32	4.78
Total	100	

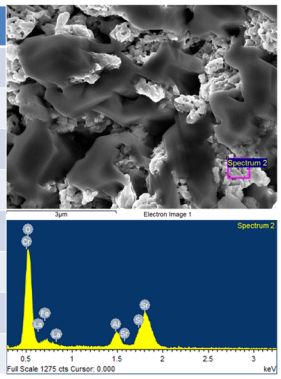

Element	Wt.%	Atomic %
La	36.29	10.40
Sr	11.55	5.25
Fe	20.05	14.29
Cr	**2.75**	**2.08**
Ba	0.79	0.23
O	28.57	67.74
Total	100	

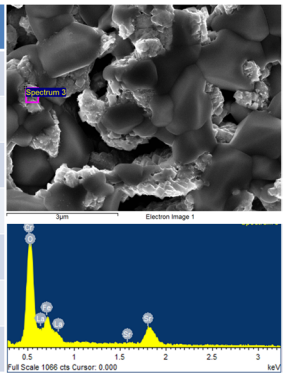

Figure 4. EDS analysis of the bare and BCO-coated LSCF after chromium contamination for 100 hour.

Figure 5 shows the electrochemical performance of BCO and various other bimetallic oxides containing barium in carbon dioxide contamination. As with the chromium conditions, BCO is shown to be an effective catalyst to stabilize LSCF in CO_2.

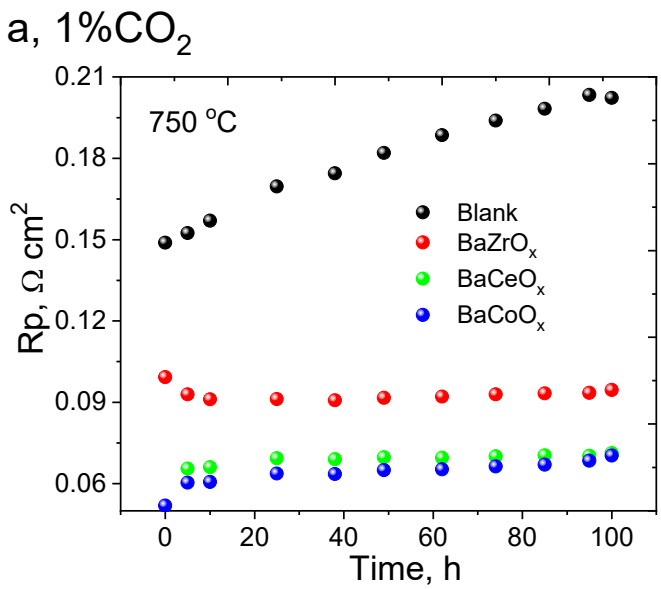

Figure 5. Long term testing of blank LSCF and LSCF coated with $BaCoO_x$, $BaCeO_x$, or $BaZrO_x$ in simulated air with 1% CO_2.

After achieving enhanced performance with BCO catalysts over the course of this project, efforts were taken to further optimize this coating. A $Ba_{0.9}Co_{0.7}Fe_{0.2}Nb_{0.1}O_x$ (BCFN) catalyst was created by doping Fe and Nb into the high performing BCO catalyst. The experimental procedures and electrochemical testing closely followed the methods previously described.

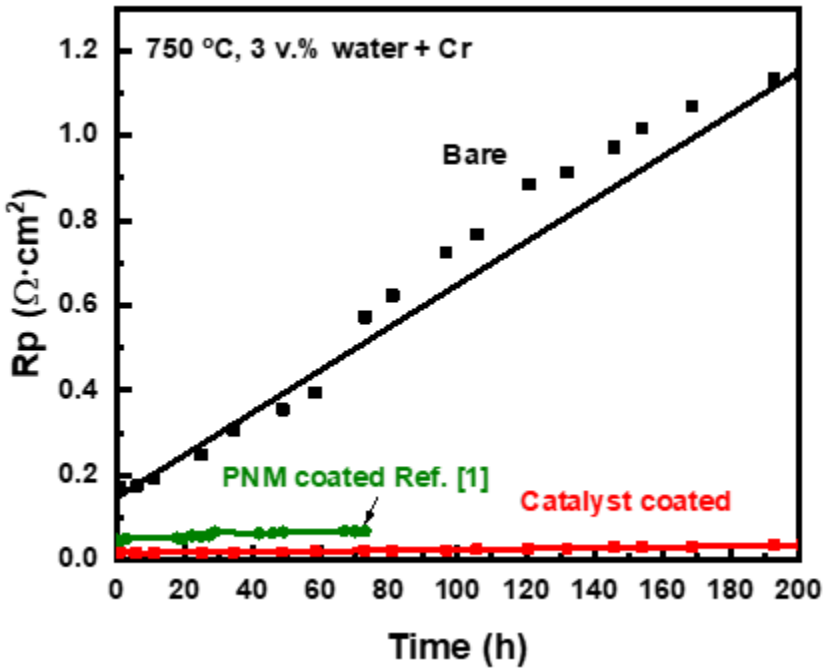

Figure 6. Polarization resistance as a function of time for bare BCFN-coated LSCF in chromium containing atmospheres showing the extreme enhancement in stability for the coated cell.

Figure 6 shows the performance of the optimized BCFN coating for 200 hours under chromium contamination. The BCFN catalyst greatly enhanced the stability of the electrode, effectively preventing degradation and chromium poisoning. Figure 7 shows the EDS analysis of the cells after chromium stability testing. The analysis shows that the BCFN coating greatly reduced the chromium present on the surface after testing. This supports the impedance data which shows great stability in the presence of chromium.

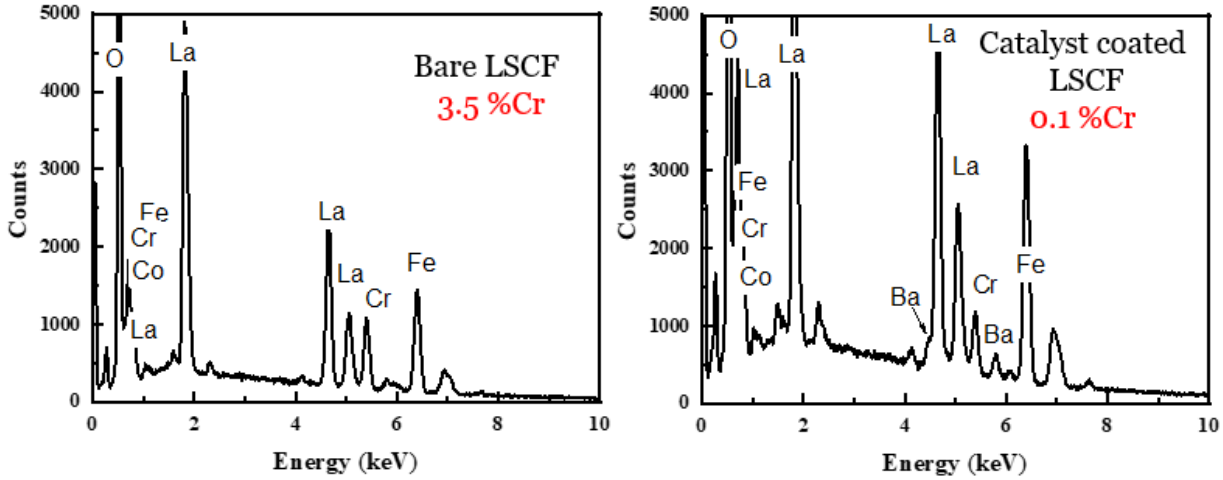

Figure 7. EDS results from the bare and BCFN-coated LSCF after 200 hours of testing in chromium containing atmospheres, showing the great reduction in chromium present on the surface of the catalyst coated cell.

Finally, the BCFN catalyst coating was applied to full cells to evaluate the catalyst in realistic conditions. Figure 8 shows the I-V-P curves for the bare and coated Ni/YSZ-YSZ full cells. It can be seen that the catalyst coating increased the maximum power density greatly from about 875 mW/cm^2 to 1.2 W/cm^2. The data show that this catalyst coating is extremely effective at decreasing the polarization resistance, increasing the stability under chromium contaminating conditions, and increasing the maximum power density.

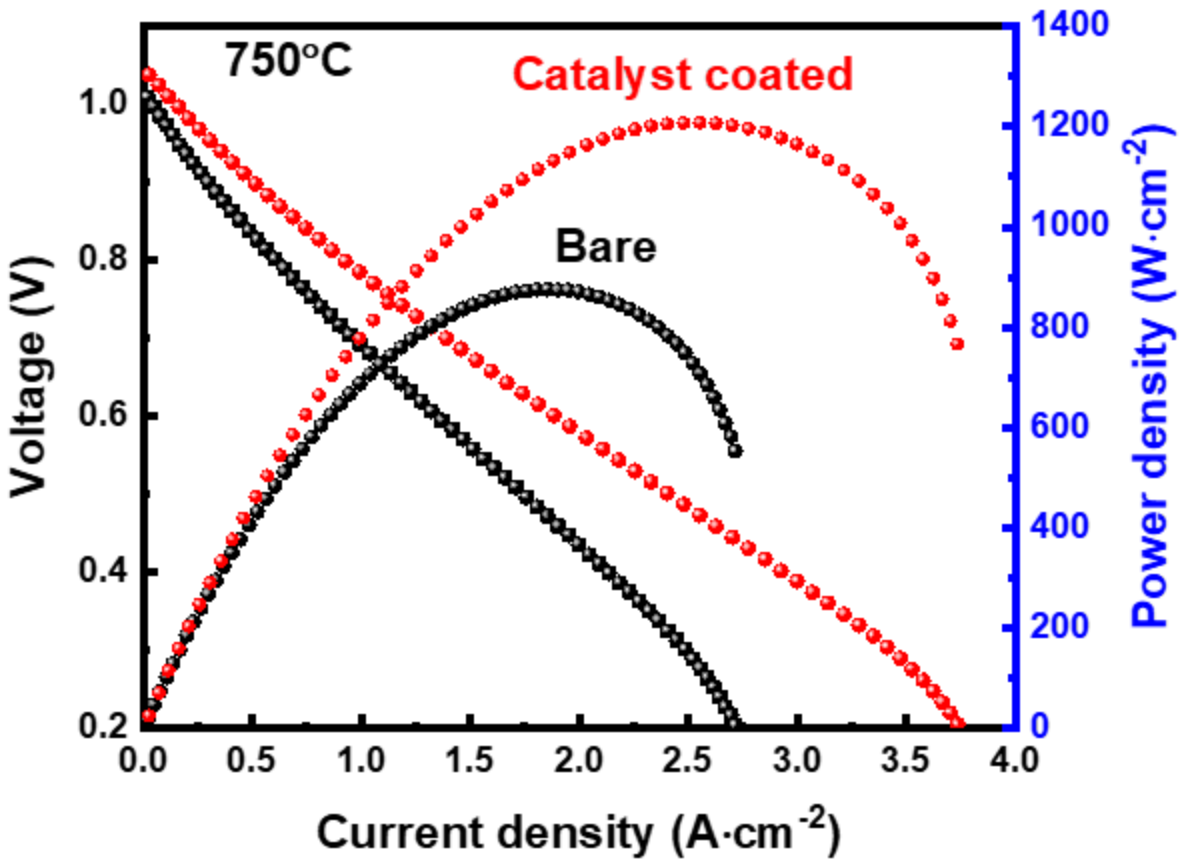

Figure 8. I-V-P curves of the bare LSCF and BCFN coated LSCF full cells.

3.2 Electrochemical Relaxation Analysis of Catalyst Coatings

In solid oxide fuel cell systems, the oxygen reduction reaction (ORR) occurs at the cathode. The ORR is the process that oxygen atoms are reduced to oxygen ions and then diffuse to the interface between cathode and electrolyte for the anodic reaction. Two processes, oxygen being absorbed through the surface and being diffused through the cathode, are strongly influenced by the surface exchange coefficient (k) and diffusion coefficient (D) of the material. In addition, it's believed that catalysts can influence the surface exchange property of a material. Thus, reliable measurements of k and D are important to determine the performance of cathode materials and catalysts in SOFC systems.

Electrical conductivity relaxation (ECR) is one powerful method that can measure the surface exchange coefficient and diffusion coefficient. It combines the surface exchange of oxygen between the cathode and gaseous oxygen in air, diffusion of oxygen atoms within the bulk cathode,

and conductivity of cathode together, to determine k and D. Generally, at the working temperature and certain oxygen partial pressure conditions, the resistance of cathode bars are measured. The oxygen partial pressure is then changed to a new condition in as quickly as possible. If the oxygen partial pressure is increased, oxygen from the atmosphere will be absorbed into the cathode material, reducing the concentration of oxygen vacancies inside the cathode. As a result, more free electrons will be generated and thus the conductivity will be higher. Likewise, the conductivity will be reduced if the partial pressure is decreased. The relative conductivity change from 0 to 1 can be recorded with time. The curve can then be fit to the equations seen in Figure 9 to calculate k and D.

$$\frac{M_t}{M_\infty} = 1 - \sum_{i=1}^{\infty}\sum_{m=1}^{\infty}\sum_{n=1}^{\infty} \frac{2L_1^2 \exp(-\beta_i^2 Dt / l_1^2)}{\beta_i^2(\beta_i^2 + L_1^2 + L_1)} \frac{2L_2^2 \exp(-\gamma_m^2 Dt / l_2^2)}{\gamma_m^2(\gamma_m^2 + L_2^2 + L_2)} \frac{2L_3^2 \exp(-\delta_n^2 Dt / l_3^2)}{\delta_n^2(\delta_n^2 + L_3^2 + L_3)}$$

$$\frac{M_t}{M_\infty} = \frac{C_O(t) - C_O(0)}{C_O(\infty) - C_O(0)} = \frac{C_{V_O^{\bullet\bullet}}(t) - C_{V_O^{\bullet\bullet}}(0)}{C_{V_O^{\bullet\bullet}}(\infty) - C_{V_O^{\bullet\bullet}}(0)} = \frac{C_{h^\bullet}(t) - C_{h^\bullet}(0)}{C_{h^\bullet}(\infty) - C_{h^\bullet}(0)} = \frac{\sigma(t) - \sigma(0)}{\sigma(\infty) - \sigma(0)} = g(t)$$

Figure 9. ECR Equations used to calculate k and D.

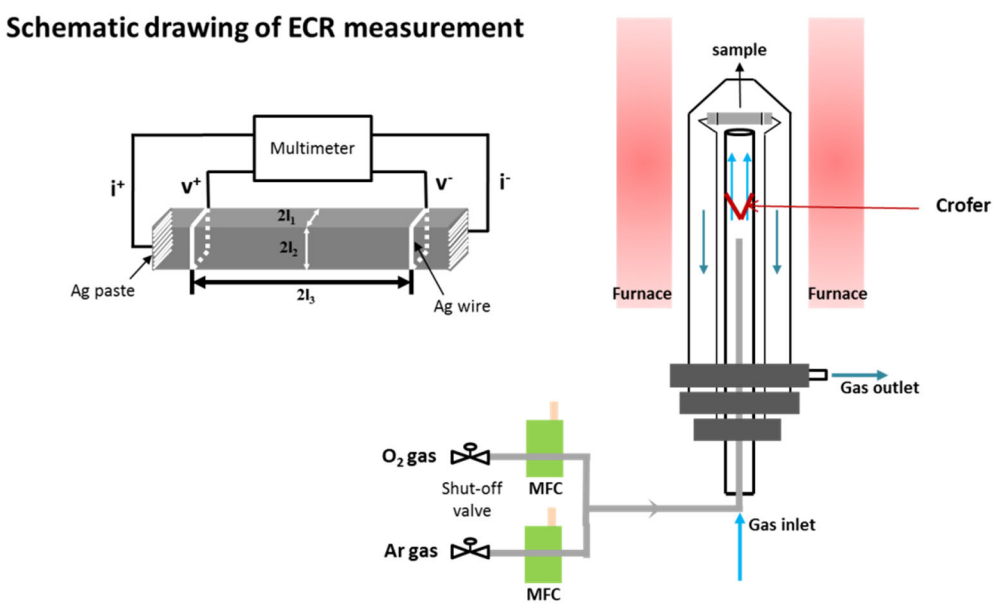

Figure 10. Schematic of the ECR measurement setup.

To perform ECR measurements, dense LSCF bars were fabricated and BCO and SCO catalyst films were deposited on the surface of the bar using RF sputtering. The effect of the catalyst coatings on the surface exchange coefficient was then examined using the ECR technique. Figure 11 shows the surface exchange coefficient for BCO- and SCO-coated LSCF as a function of temperature and catalyst thickness. For both catalysts, an optimum thickness achieving the

highest surface exchange coefficient is observed around 100 nm, after which increasing the thickness results in a stable (BCO) or decreasing (SCO) surface exchange coefficient.

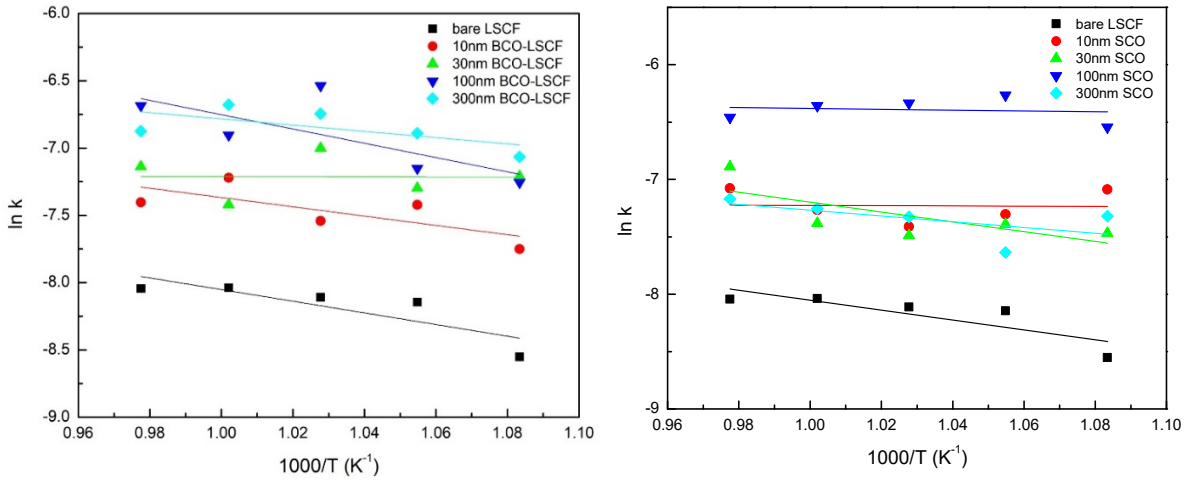

Figure 11. Surface exchange coefficient (k) as a function of catalyst thickness and temperature for (a) BCO- and (b) SCO-coated LSCF.

3.3 Fundamental Investigation of Catalysts Coatings using Model Cells

Model cells were utilized to investigate the fundamental reaction mechanisms and the effect of the catalyst coatings. The model cell is an asymmetric cell consisting of one standard porous LSCF electrode and one fully dense LSCF electrode. The dense electrode forces the electrochemical reactions to occur on the two phase boundary between the LSCF and the air, as opposed to the triple phase boundary. The two phase boundary is readily observable since it is on the surface of the dense electrode, as opposed to the triple phase boundary which is hidden under a porous electrode. This allows for observation of the electrochemical reactions and products with Raman spectroscopy and SEM. In addition, the reduced surface area of the dense electrode causes the impedance spectrum to be dominated by the resistance of the dense electrode, allowing for changes to be attributed to coatings on the dense electrode.

In brief, the model cell's dense electrode was fabricated by RF Sputtering. The standard process to fabricate a symmetrical cell was used to fabricate the electrolyte and one porous electrode, however, the dense electrode was sputtered onto the polished electrolyte surface instead of using a second LSCF tape. The electrolyte and dense LSCF film can be seen in Figure 12. In order to investigate the effect of catalyst coatings, catalyst films were sputtered on the surface of the dense electrode.

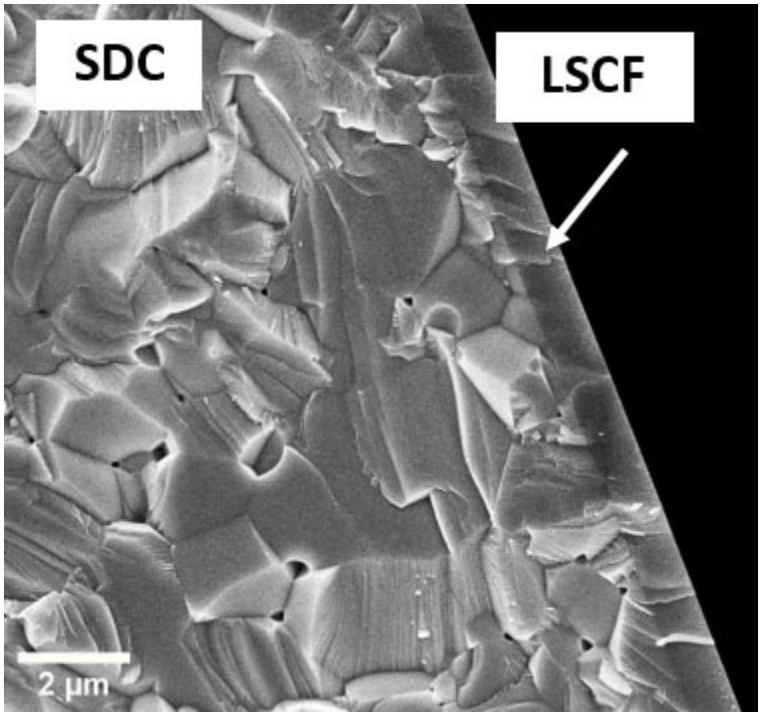

Figure 12. Cross sectional SEM image of the dense electrode, showing the SDC electrolyte and dense LSCF film.

Figure 13 shows the electrochemical performance of the bare and BCO-coated model cells in CO_2 and chromium containing atmospheres. The model cell performance closely matches the trends observed in the symmetrical cells, validating the model cell design.

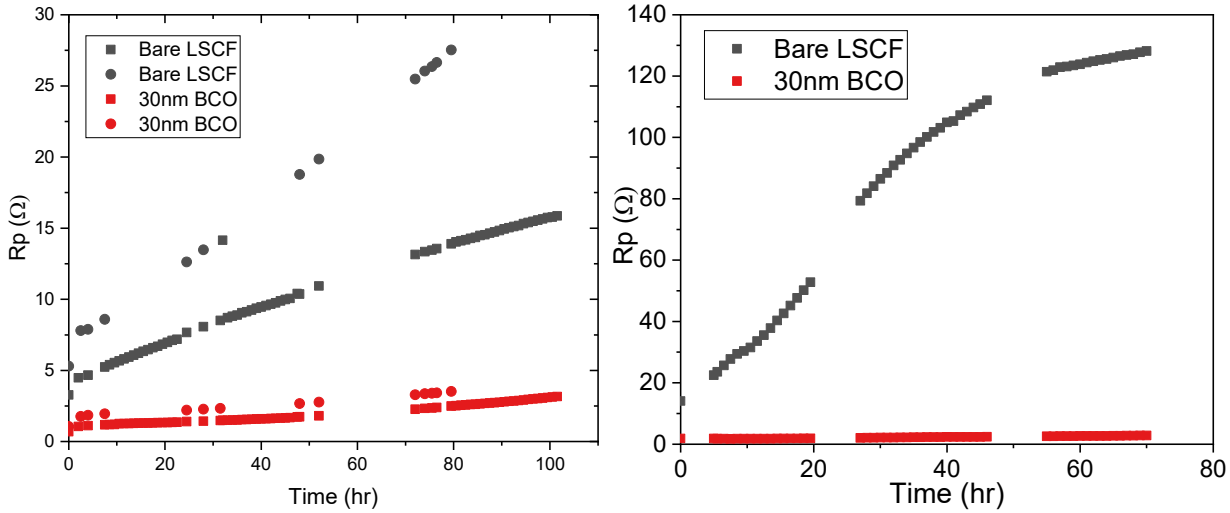

Figure 13. Polarization resistance versus time for model cells under (a) 3% CO2 and (b) indirect Cr contamination conditions showing the reduction in degradation for the BCO coated cells.

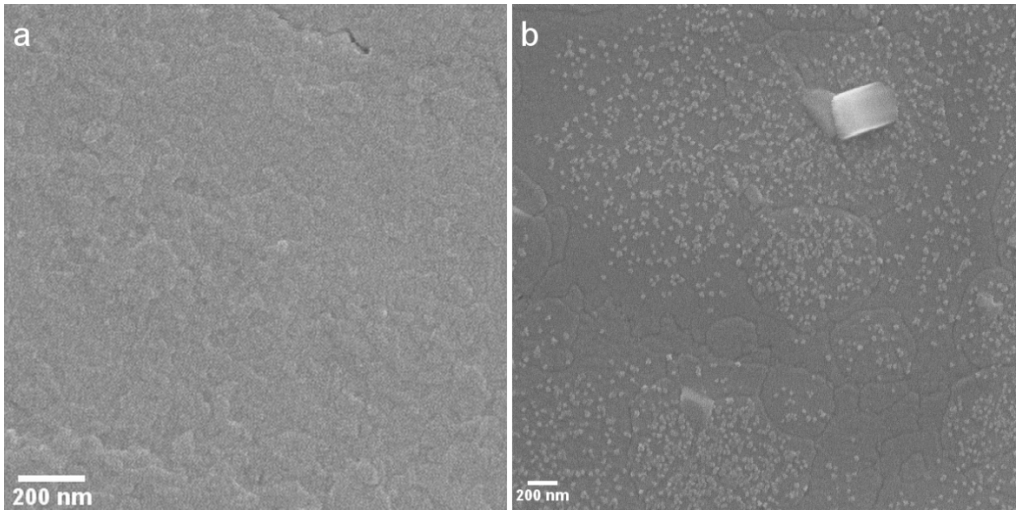

Figure 14. SEM images of the surface of the dense electrode for the (a) bare LSCF and (b) 30 nm BCO cells after 100 hours of 3% CO_2 contamination conditions showing the presence of particulates on the surface.

Ex-situ analysis was performed on the model cells after the contamination stability tests. Figure 14 shows SEM images of the surface of the dense LSCF electrode after testing in CO_2 contamination. The images show significant film formation on the surface of the uncoated LSCF electrode, while the BCO coated electrode shows the formation of significantly fewer particles. This is supported by the Raman analysis, shown in Figure 15, which observed the presence of carbonate on the surface of the bare electrode, while no significant carbonate peak is observed on the BCO-coated electrode. For the chromium contamination, Raman spectroscopy, seen in Figure 16 and Figure 17, proved the formation of insulating Cr_2O_3 and $SrCoO_4$ on the bare cell, while the BCO coated cell formed electrically conductive $BaCrO_4$. The stability improvements in chromium containing atmospheres is attributed to the formation of this electronically conducting phase over insulating phases.

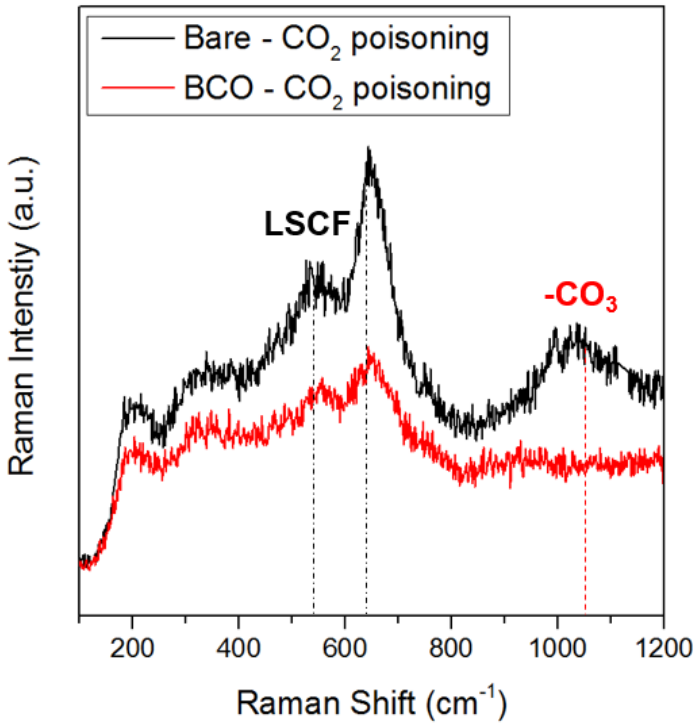

Figure 15. Raman Spectra of the bare and 30nm BCO coated model cell showing the formation of carbonate on the surface the cell after testing in carbon dioxide contamination conditions.

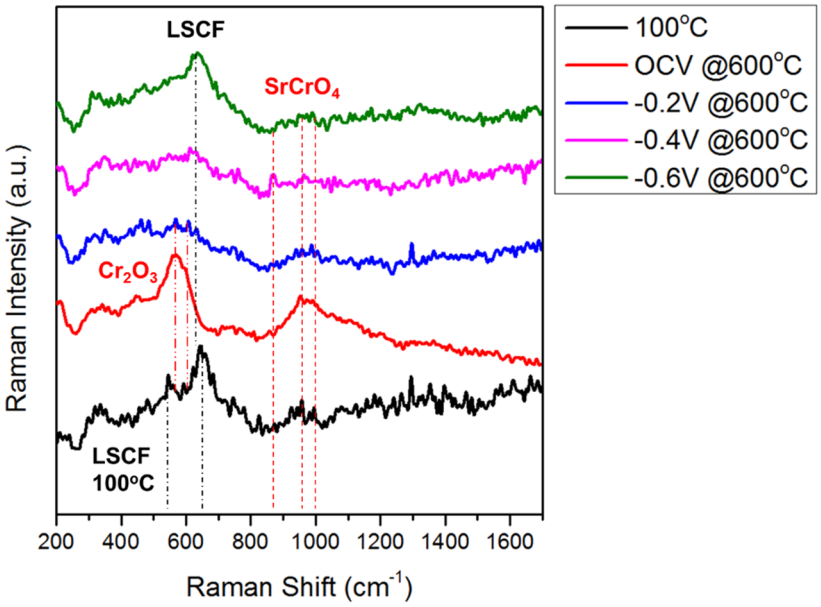

Figure 16. Operando Raman spectroscopy analysis of the LSCF model electrode with Cr-poisoning at different cathodic bias showing the evolution of $SrCoO_4$ and Cr_2O_3 phases.

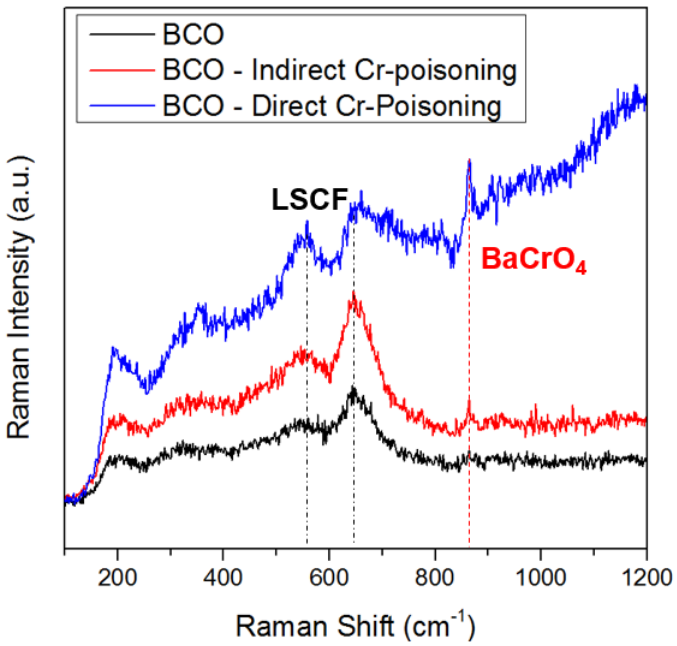

Figure 17. Raman Spectra of the 30 nm BCO coated model cell showing the formation of BaCrO4 on the surface the cell after testing in Cr contamination conditions.

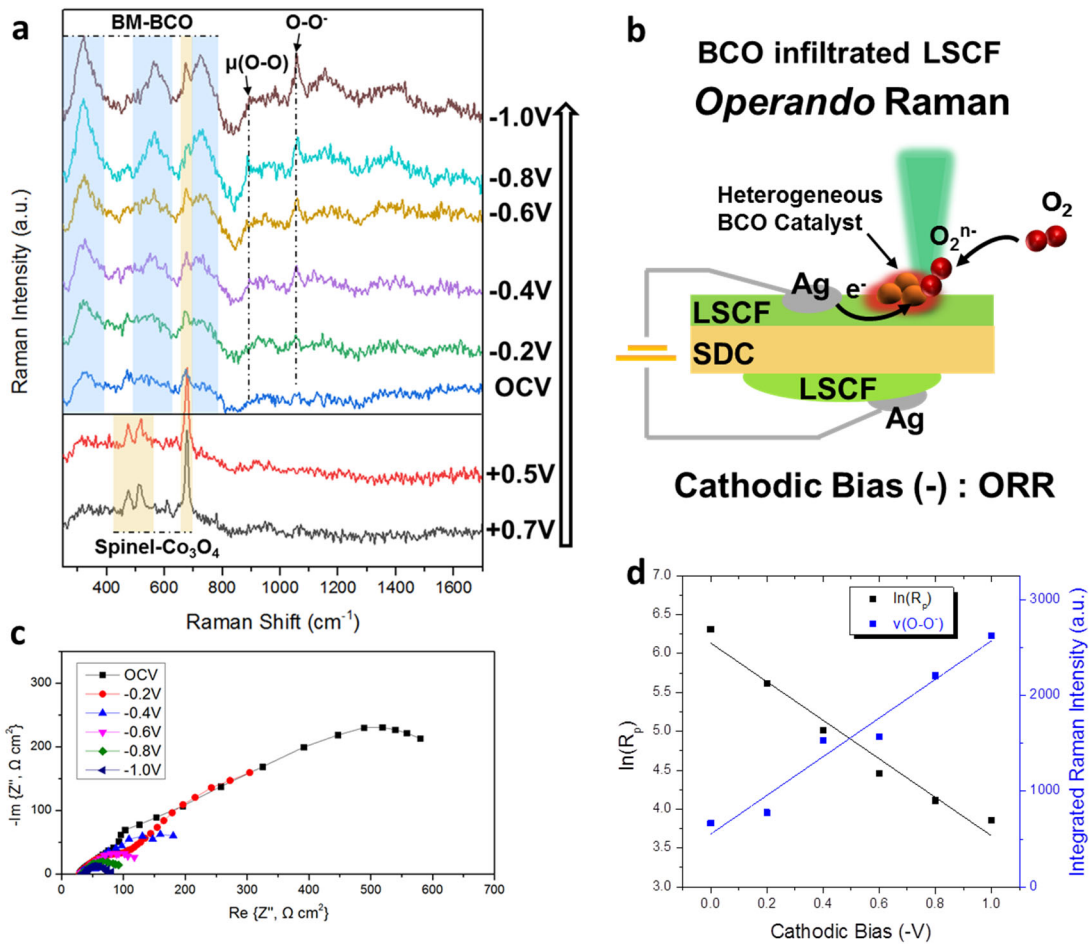

Figure 18. (a) Operando Raman spectroscopic evolution of BCO catalyst surface at 600 °C with 1 atm O_2 atmosphere (b) Schematics for operando Raman spectroscopy set-up with BCO infiltrated LSCF model cell coupled with impedance spectroscopy. (c) Resulting impedance spectroscopy (d) Quantitative correlation between Raman intensity of superoxo-like species and polarization resistance.

To gain a fundamental understanding, one important step forward is to carefully examine the heterogeneous surface of the BCO catalyst. Thereby, surface-sensitive *operando* Raman spectroscopy analysis is conducted to assess the surface chemistry of the BCO catalyst under conditions relevant to SOFC cathodes. Uniquely designed model cells with a dense LSCF electrode is coated with BCO catalyst. The model cell was placed in an *operando* Raman spectroscopic chamber with electrical connection for impedance spectroscopy and a chamber temperature of 600°C with 1 atm O_2 (Figure 18b).

As shown in Figure 18a, BCO shows a flexible oxygen stoichiometry between anodic to cathodic sweeping. In anodic sweeping, three Raman active phonon modes attributed to the spinel structure (Co_3O_4) can be found, E_g (487 cm^{-1}), F_{2g} (529 cm^{-1}), and A_{1g} (692 cm^{-1})[29]. On the other hand, transition into brownmillerite (BM)-like phase $BaCoO_{2.5}$ (320 cm^{-1}, 564 cm^{-1}, 727 cm^{-}

^{1}) can be detected in cathodic sweeping[30]. This result manifests that BCO will turn into a phase with more oxygen vacancies to occupy favorable ORR kinetics. Along with a phase transition, a new band at 1057cm^{-1} is gradually seen with cathodic bias. Active oxygen intermediates are reported with vibrational spectroscopy in a regime of 800-1150 cm^{-1} [31, 32], and Hsin-Yi et al., recently reported superoxide moieties at 1068cm^{-1} with Co_3O_4 electro-catalyst[33]. Therefore, we assigned the newly evolved band as active superoxo-like species which should be a key participant in ORR pathways of BCO catalysts. With further increase of bias, an additional band at 889cm^{-1} can be identified. In ORR pathways, superoxo-like species will be further reduced into peroxo-like species (μ(O-O)) with more negative charges thus the O-O distance is further stretched, accompanied by red shift of vibrational frequency [34, 35]. Because peroxo-like species have been identified in the wavenumber region of 886-936cm^{-1} [33, 34], it is reasonable to assign newly developed 889cm^{-1} band as a peroxo-like species resulting from reduction of super-oxo like species (1057cm^{-1}). The characteristic active oxygen intermediate bands with strong intensity imply the active role of BCO catalyst with reference to ORR. The extraordinary oxygen uptake capability of BCO nanoparticles was also addressed by Density Functional Theory calculation due to the presence of large amount of surface oxygen vacancies[36].

However, if surface intermediates analysis is not well-correlated with electrochemical polarization of the cell, the interpretation of spectroscopic evolution can be elusive. To avoid certain issues, the model electrode performance was recorded with impedance spectroscopy with synchronized spectroscopic evolution (Figure 18c-d). By generating quantitative correlation between vibrational features with polarization of the electrode, we deliver substantial information that BCO-modified LSCF surface polarization decreases in a logarithmic scale with linear increment of super-oxo like species. Thereby, it is now unambiguous that heterogeneous BCO catalyst decoration facilitates active oxygen adsorptions, which results in advanced electrochemical performance.

3.4 Atomic-level understanding of contaminates-tolerance enhancement

$PrBa_{0.8}Ca_{0.2}Co_2O_{5+\delta}$ (PBCC) demonstrated superior contaminant tolerance against $Cr(OH)_2O_2$, CO_2, H_2O and SO_3. However, the atomic level mechanism needs to be understood so that a rational design of better materials can be performed. For this computational analysis, density functional theory calculations were utilized to gain insight into the thermodynamic stability of PBCC when exposed to the contaminant molecules, including the thermodynamics for adsorption

of contaminant molecules on the PBCC (001) surface. These analyses provide us with the energetic criteria for secondary-phase formation and surface adsorption.

The bulk phase stability was investigated using a thermodynamic analysis. A supercell of bulk PBCC consisting of 40 atoms was constructed. Various reactions between the PBCC and contaminates were written, allowing for a thermodynamic calculation of the gibbs free energy. The 0K electronic energy, ΔE_{0K}, of four contaminants is shown in Figure 19. The Cr-based contaminant has the most negative reaction energy (~-5.5 eV/formula), indicating it is more severe than the other contaminants. The 0K reaction energy magnitude has the order of $CrO_2(OH)_2 < SO_3 < CO_2 < 0 < H_2O$. Interestingly, water contamination through a bulk reaction is energetically unfavorable at 0K. The thermodynamic analysis in the presence of $CrO_2(OH)_2$ indicates that the ΔG values for both PBC and PBCC are very negative, mostly due to a very negative ΔE_{0K} indicating a very strong contamination driving force.

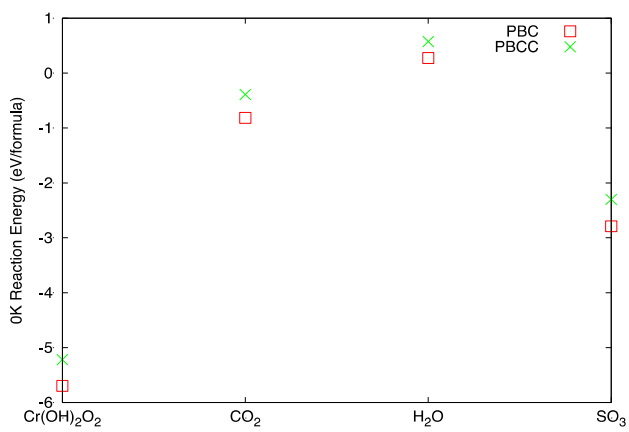

Figure 19. Reaction energy (in eV/formula at 0k) for bulk PBC (dot-in-red-square) and PBCC (green cross).

The thermodynamic analysis in the presence of SO_3 indicates that PBC and PBCC have very similar slopes for their ΔG curves. The only difference is from ΔE_{0K}, where PBCC shows better stability than PBC at 0K. SO_3 is less severe than Cr.

The thermodynamic analysis in the presence of H_2O gives distinct ΔG curves for PBC and PBCC. In terms of stability, both materials have a very good starting point, i.e. near zero. However, $\Delta S_{T,0K}$ for PBC is very positive, and for PBCC it is near zero. This difference is believed to be from $Ca(OH)_2$, the only elementary difference between PBCC and PBC. As observed, $Ca(OH)_2$ has a layered structure, while $Ba(OH)_2$ has a 3D crystal structure with the hydrogen bond

network. Based on this result, PBCC performs excellently against H_2O contamination, while PBC is even less stable against H_2O than SO_3.

The thermodynamic analysis in the presence of CO_2 suggests that both materials have excellent stability. Due to a slight entropic difference, PBC has better stability than PBCC at high temperatures. This Gibbs free energy cross-over occurs at ~900K.

In conclusion, both materials have the best stability against CO_2, followed by H_2O and SO_3. Due to the special layered calcium hydroxide structure but conventional 3D structure of barium hydroxide, the entropic factor severely destabilizes PBC w.r.t PBCC. Cr contamination is the most severe one among all four contaminants.

3.5 Advanced Deposition of Catalyst Coatings using Surface Sol-gel

Surface sol-gel was utilized in order to coat catalyst films on porous electrodes. This process utilizes liquid phase alkoxide precursors that chemisorb to the surface of the substrate, which are then subsequently hydrolyzed to form an oxide coating. Conceptually, this process is essentially ALD performed in the liquid phase as opposed to the gas phase.

The surface sol-gel process, shown schematically in Figure 20, can be described in two main steps; the first is chemisorption of a metal alkoxide to the substrate surface. The following step is aqueous hydrolysis of the chemisorped layer to form an oxide. The metal alkoxides used in the first step are highly reactive towards nucleophilic reactions. Thus, native surface hydroxide groups exposed to the metal alkoxide quickly react, bonding the metal to the oxygen and liberating a 2-propanol molecule. Just as ALD reactions are self-limiting, once all the hydroxide groups have reacted, no more precursor can react with the surface. The second step involves a condensation reaction, liberating the remaining isopropoxide ligands from the cation and forming new hydroxide groups. By alternating solutions, the coating can be built up layer by layer. Thus, this process generates conformal coatings with precise thickness control by adjusting the number of cycles.

The surface sol-gel process was carried out by a custom-built computer-controlled robot, capable of dispensing precursor solutions, sonicating and draining the reaction vessel, and drying the sample. The robot consists of multiple peristaltic pumps, which can pump precursor fluids into the reaction vessel. The reaction vessel is a medium porosity fritted glass Buchner funnel, which is ideal for this process because vacuum is required for liquid to drain through the fritted glass. Thus, the vessel can be filled with precursor solution to soak the sample, and then a vacuum can quickly drain the vessel. A stopcock attached to the bottom of the Buchner funnel controlled by a

servo performed this draining action by connecting the vessel to a vacuum pump. The reaction vessel is submerged in a sonicating bath in order to sonicate the samples during the soaking and rinsing. A heat gun is pointed into the reaction vessel to dry the samples between cycles. Precursor solutions were prepared in an argon glove box to prevent reaction with moisture. Nitrogen purge gas was pumped into the precursor bottles in order to prevent reaction with moisture in the ambient air.

Previously, barium oxide has shown to be an excellent catalyst for LSCF, thus it was the focus of the surface sol-gel deposition. The barium precursor used was 20w/v barium isopropoxide in isopropanol (Alfa Aesar). The solution was diluted to 15 mM using anhydrous 2-propoanol (Alfa Aesar). 40 vol% IPA in DI water was used as the second precursor. Anhydrous 2-propanol was used as the rinse solvent.

LSCF symmetrical cells were first fabricated using previously described methods. In order to clean the surface and increase the density of surface hydroxide groups, cells were cleaned under oxygen plasma for 30 minutes. To coat the cells, they were first placed in the reaction vessel, resting on the fritted glass. 15 mM barium isopropoxide precursor was pumped into the vessel to fully submerge the samples. The cells were allowed to soak for 3-5 minutes in order to allow for full adsorption of the coating. Sonication was applied to the cells while they soaked. Then the precursor solution was drained through the fritted glass and the samples were submerged in an anhydrous IPA rinse, in order to remove any physisorped precursor. After 30 seconds of sonication in the rinse, the rinse was drained and new rinse was added. This rinse process was repeated one more time for a total of three rinses. After the third rinse, the sample was submerged in the water precursor for 1 minute to complete the condensation reaction. Then the sample was rinsed three more times using the same process as above. Then the sample was dried for 2 minutes using room temperature air from the heat gun. This completes one cycle. The process was then repeated for n cycles.

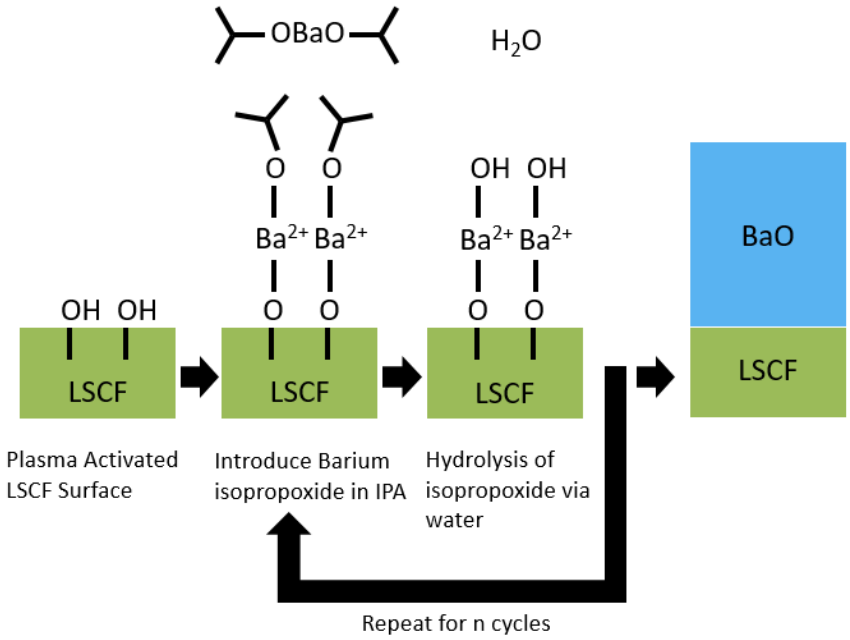

Figure 20. Schematic of the layer-by-layer surface sol-gel process, demonstrating the deposition of BaO with barium isopropoxide.

The number of deposition cycles was varied in order to determine the optimal thickness of the SSG catalyst coating. Figure 21 shows the polarization resistance as a function of time for various coating thicknesses. This figure shows that there is an optimum thickness achieved at around 15-50 cycles. It can be seen that while 5 cycles provides good initial catalytic activity, the cell begins to experience degradation indicating the coating is too thin. 15 to 50 cycles all provide similar results, both reducing the initial polarization resistance and preventing degradation over the duration of the test. For the 70 cycle coatings, a larger polarization resistance is seen. This indicates the coating has passed the optimal thickness, and the lower ionic conductivity of the catalyst is increasing the overall cell resistance. Thus the optimum thickness is seen at around 30 cycles, providing good catalytic activity while also providing good durability over time.

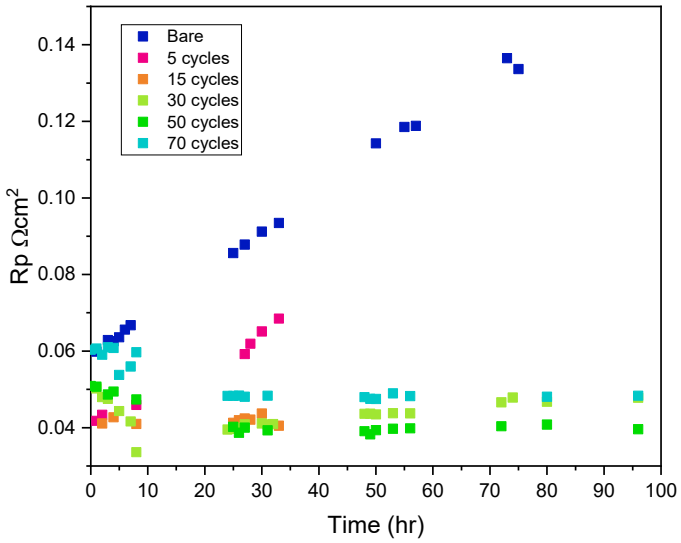

Figure 21. Polarization resistance versus time for LSCF cells coated with 0, 5, 15, 30, 50, and 70 cycles of BaO at 750 °C.

The developed SSG process was applied to large diameter symmetrical cells to demonstrate the ability to scale the process. These cells were then tested in chromium poisoning conditions to determine the stability of the cell and catalyst coating. As shown in Figure 22, the BaO SSG coating greatly improved the performance of the cell during the 200 hours tested. After the initial activations, the bare cell degraded at a rate of 0.00613 Ωcm^2/hour, while the catalyst coated cell had an effective rate of 0 Ωcm^2/hour over 200 hours.

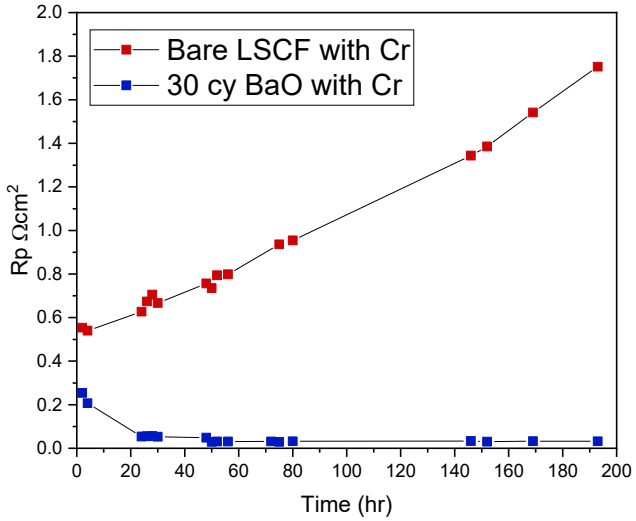

Figure 22. Polarization resistance versus time for 30 mm LSCF symmetrical cells in 3%H_2O+Air+Crofer 22 at 750°C for 200 hours.

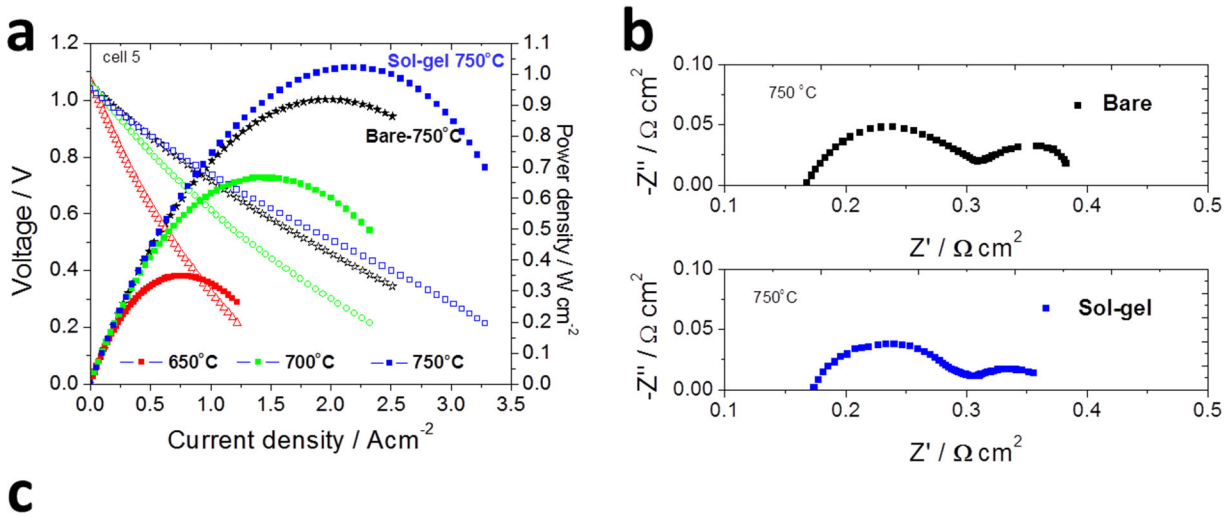

c

Cathode	Pmax@750°C	Rp@750°C
LSCF	0.9 Wcm^{-2}	0.21 Ωcm^2
BaO-LSCF (sol-gel)	1.05 Wcm^{-2}	0.18 Ωcm^2

Figure 23. (a) Typical I-V-P and (b) EIS curves of single cells with LSCF cathodes modified by a surface sol-gel coating and blank LSCF; (c) Comparisons of performance of single cells with bare LSCF and LSCF with surface sol-gel coating.

The surface sol-gel process was also applied to full cells. Figure 23 shows the typical IVP curves and the impedance spectra for the cells with bare and BaO-coated LSCF cathode measured at 750 °C under OCV conditions. The total polarization resistance of the cell is shown to decrease with the addition of the catalyst coating, as seen in the symmetrical cell data.

The surface sol-gel coatings support the conclusions from the solution infiltration experiments. BaO catalyst coatings have shown to be extremely effective at reducing degradation due to contaminates in the gas stream. The surface sol-gel process developed during this project has shown to be an effective method of applying BaO catalyst to porous electrodes.

3.6 Demonstration of Catalyst Coatings on Full Cells

The final focus of the project was to demonstrate the optimized coatings developed over the course of this project on full fuel cells. Ni/YSZ|YSZ|LSCF standardized cells with a stable baseline performance were fabricated with commercial materials. The previous catalyst solution infiltration process developed for 10 mm cells was applied to large full cells. Two different infiltration catalysts were used: $BaCoO_{3-\delta}$ (BCO) and PBCC. Figure 24 shows the surface of the full cell cathode before and after infiltration.

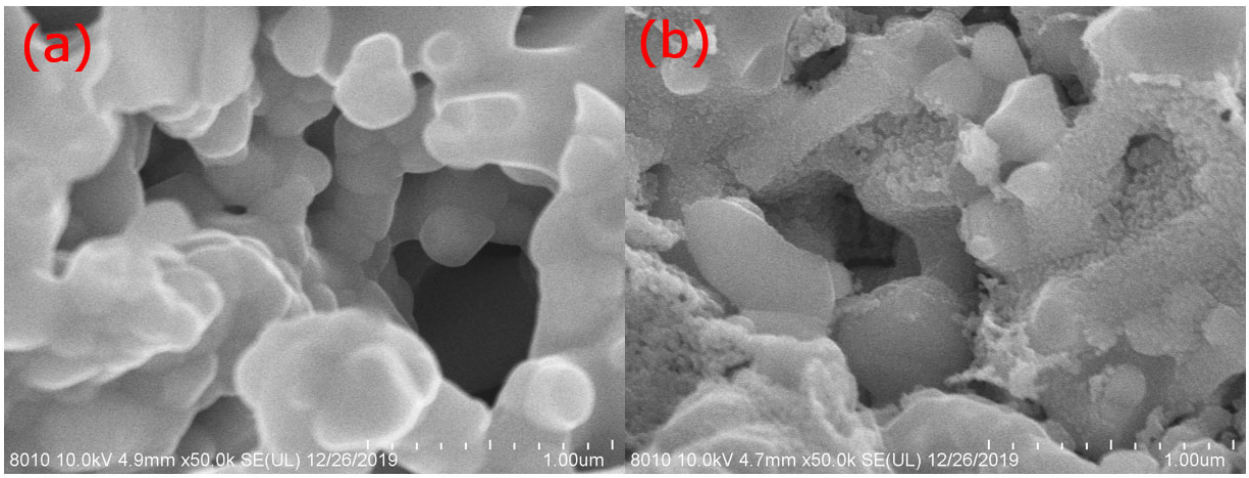

Figure 24. SEM images of the (a) bare LSCF surface and (b) BCO coated LSCF surface after firing.

Figure 25 shows the IVP curves and impedance spectra for the bare and BCO coated full cells in air at 700 °C. The catalyst coating increased in maximum power density, attributed to a lower polarization resistance, seen from the impedance spectra.

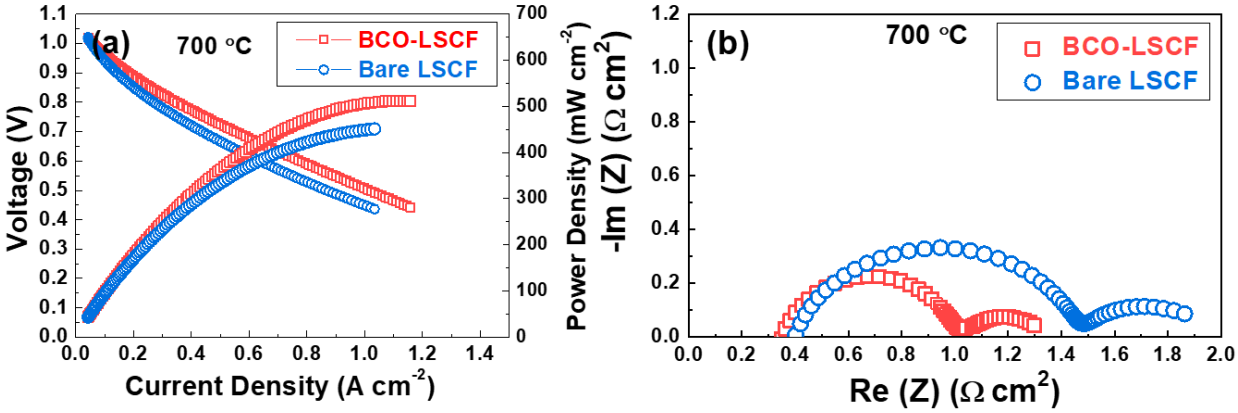

Figure 25. (a) IVP curves and (b) impedance spectra of bare LSCF and BCO-modified LSCF full cells at 700 °C, showing the enhancement from the surface modification.

Figure 26 shows the tolerance to chromium contamination induced by Crofer 22 and 3% H_2O in the cathode's air supply. Cell #1 shows the performance of the bare LSCF full cell without chromium contamination and represents degradation methods not associated with chromium poisoning. Cells #2-1 and 2-2 show the tolerance of the BCO-modified LSCF under chromium poisoning conditions, which show great stability, nearing the performance and degradation rate of the uncoated and non-poisoned cell. In contrast, cell #3 shows the uncoated cell exposed to chromium poisoning conditions. It is clearly seen that the uncoated cell suffers great current density losses and experiences a greater degradation rate due to the chromium poisoning. The calculated degradation rates verify the visual conclusions from Figure 26. The BCO modified cells

under chromium poisoning show a degradation rate of 0.052%/h and 0.11%/h, compared to a degradation rate of 0.086%/h for cell #1 without modification or contamination. In contrast, the unmodified cell experienced a degradation rate of 0.31%/h, which is about 3 times higher than the modified cells. Thus, the full cell data verifies conclusions made in previous reports showing that BCO surface modification of LSCF greatly reduces chromium poisoning. These results demonstrate that the BCO surface modification is also applicable to full cells by greatly reducing the degradation experienced in chromium poisoning conditions.

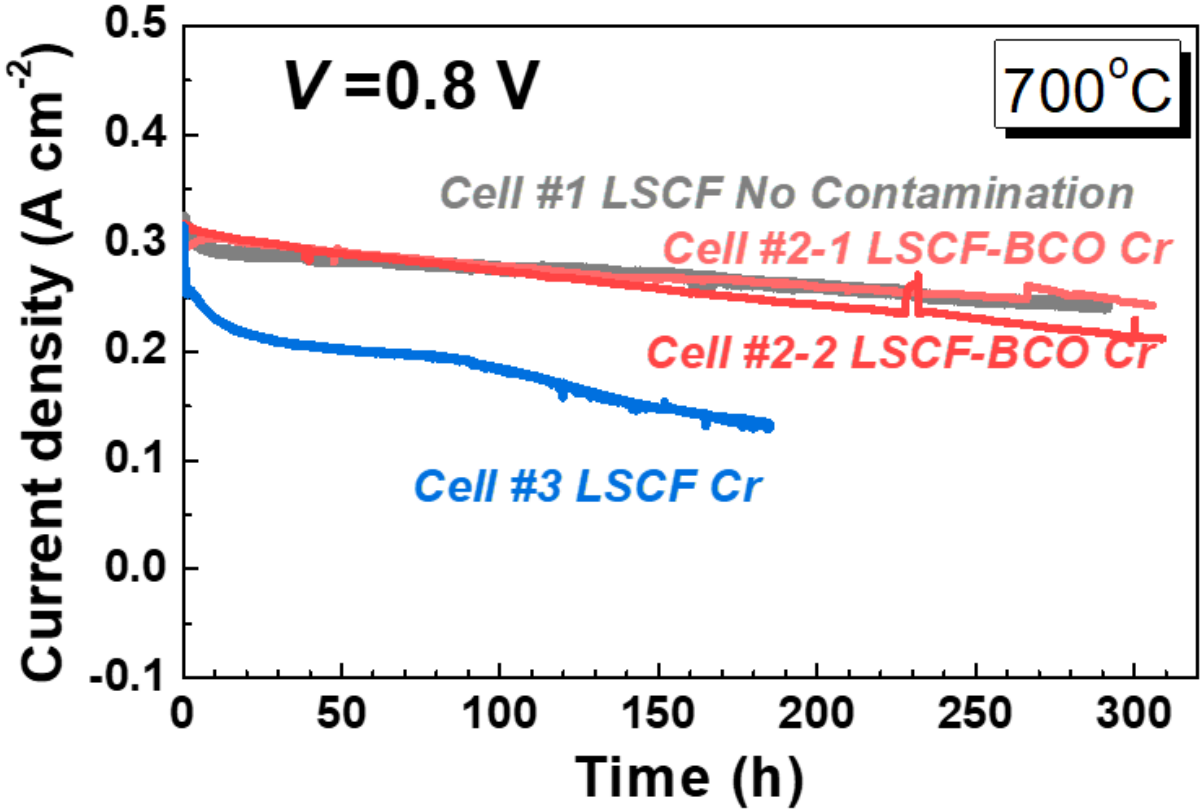

Figure 26. Current density versus time curves for various LSCF full cells potentiostatically held at 0.8V showing the tolerance to chromium contamination from Crofer 22 and 3% H_2O in the cathode's air supply at 700 °C.

Cells were also investigated for their tolerance to carbon dioxide. PBCC was chosen as the catalyst modification for carbon dioxide studies as it has previously shown good stability in CO_2 containing atmospheres. Figure 27 shows the current density versus time for potentiostatic tests of various full cells at 700 °C. The baseline unmodified cell without contamination is again shown as cell #1. Cell #2 and 3 are the PBCC-modified and unmodified LSCF full cells in 8% CO_2 contamination, respectively. The enhancement of the PBCC catalyst coating can clearly be seen

from Figure 27, where the PBCC-modified cell under CO_2 contamination generated a higher current density over the baseline cell. In contrast, the unmodified cell experienced severe degradation due to the carbon dioxide present at the cathode. The calculated degradation rates between hours 10 and 290 demonstrate the surface modification's improvement, as the PBCC modified cell experienced a degradation rate of 0.02 %/h, far lower than the 0.14 %/h experienced by the unmodified cell. In addition, the catalyst modification increased the current density of the cell under contamination to higher than that of the unmodified cell without contamination, showing the catalytic improvement of the surface modification. These results demonstrate the effectiveness of the PBCC catalyst infiltration to increase activity towards ORR and decrease the degradation rate.

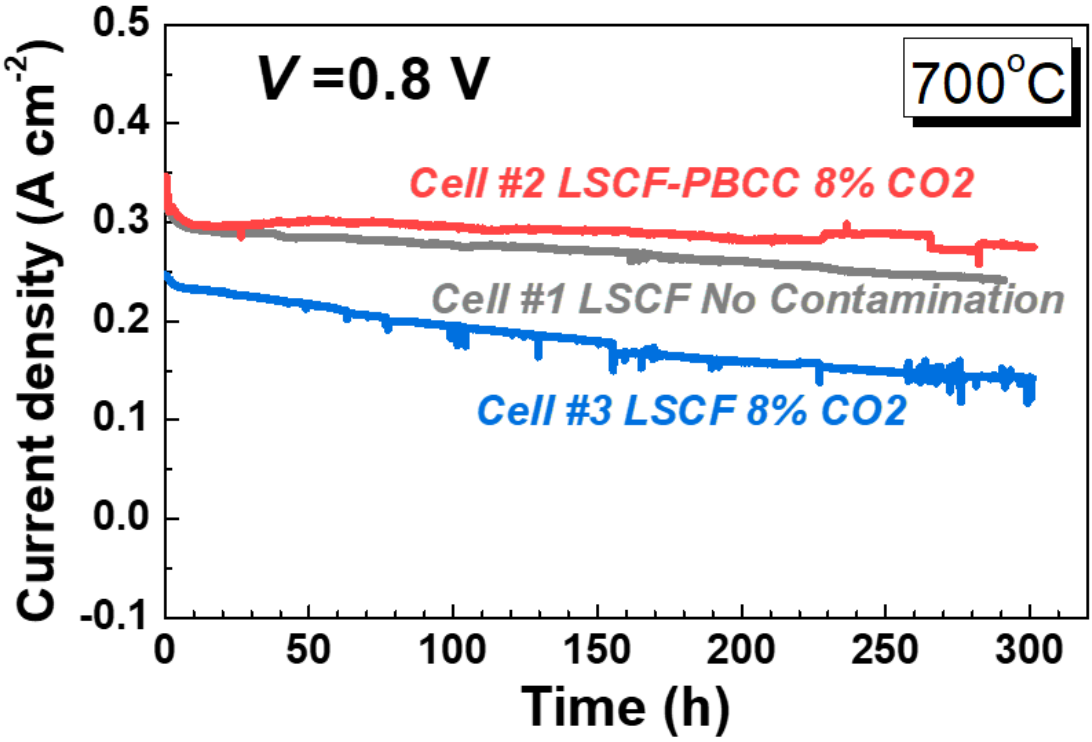

Figure 27. Current density versus time curves for various LSCF full cells potentiostatically held at 0.8 V showing the tolerance to CO_2 contamination in the cathode's air supply at 700 °C.

The results presented in this section demonstrate the final performance enhancements developed over the course of this project. The most optimal solution infiltration modifications developed during the initial phases of this project have been applied to full cells and tested under contamination conditions for over 250 hours of continuous use. The results shown demonstrate the effectiveness of the catalyst infiltrations to increase activity towards ORR while also decreasing

the degradation of the cell under chromium and carbon dioxide contamination. These results represent the culmination of the investigation.

4. Conclusions

The surface modifications developed throughout this project have increased both the activity and durability of state-of-the-art LSCF cathodes. A large variety of alkaline earth-based catalysts were screened, identifying promising avenues for further exploration. BCO and SCO were identified as high performing catalysts, and their activity and durability were demonstrated on both symmetrical cells and full cells for over 250 hours of operation in CO_2 and Cr containing atmospheres. Furthermore, a complex catalyst, BCFN, was developed and demonstrated extreme tolerance to chromium poisoning. A fundamental investigation into the electrode degradation methods was performed on model cells. The microstructural and compositional evolution of these cells was evaluated with SEM, EDS, and Raman spectroscopy, allowing for correlation between the microstructure, electrochemical performance, and the degradation of the cell. Electrochemical relaxation measurements were applied to investigate the surface exchange coefficient for catalyst coated LSCF, determining an optimal coating thickness of 100 nm. Atomistic calculations also provided a fundamental insight into the stability of PBCC electrodes and catalysts, showing thermodynamic stability to carbon dioxide poisoning, which has been verified in full cell stability tests. Additionally, a promising new surface sol-gel deposition technique has been applied to fuel cells for the first time, demonstrating improvements on solution infiltration and opening a new potential avenue for the development of SOFC catalysts. In all, this project has combined fundamental investigation and rational design to develop durable, active catalysts, demonstrating excellent activity and stability. The results have helped to advance fuel cells towards commercialization and paved the way for new SOFC catalyst advancements.

Acronyms

SOFC: solid oxide fuel cell

YSZ: yttria-stabilized zirconia

SDC: samarium doped ceria with chemical formula $Sm_{0.2}Ce_{0.8}O_{1.95-\delta}$

LSM: the cathode material with chemical formula $La_xSr_{1-x}MnO_{3-\delta}$

LSCF: the cathode material with chemical formula $La_{0.6}Sr_{0.4}Co_{0.2}Fe_{0.8}O_{3-\delta}$

PBCC: $PrBa_{0.8}Ca_{0.2}Co_2O_{5+\delta}$

SSC: the cathode materials with chemical formula $Sm_{0.5}Sr_{0.5}CoO_{3-\delta}$

LCC: the cathode material with chemical formula $La_{0.4875}Ca_{0.0125}Ce_{0.5}O_{2-\delta}$

PNM: the cathode material with chemical formula $Pr_2Ni_{1-x}Mn_xO_{4-\delta}$

XRD: x-ray diffraction

SEM: Scanning electron microscopy

TEM: Transmission electron microscopy

SERS: surface enhanced Raman spectroscopy

XAS: x-ray absorption spectroscopy

XANES: x-ray absorption near-edge spectroscopy

OCV: open circuit voltage

ORR: oxygen reduction reaction

R_p: interfacial polarization resistance

SCO: $SrCoO_{3-\delta}$

BCO: $BaCoO_{3-\delta}$

BCFN: $Ba_{0.9}Co_{0.7}Fe_{0.2}Nb_{0.1}O_x$

ECR: Electrical conductivity relaxation

SSG: Surface sol-gel

Publications

1. Y. Chen, B. deGlee, Y. Tang, Z. Wang, B. Zhao, Y. Wei, L. Zhang, S. Yoo, K. Pei, J. Kim, Y. Ding, P. Hu, F. Tao, M. Liu, "A Robust Fuel Cell Operated on Nearly Dry Methane at 500C Enabled by Synergistic Thermal Catalysis and Electrocatalysis", ***Nature Energy***, 3, 1042–1050 (2018) | https://doi.org/10.1038/s41560-018-0262-5.
2. Yu Chen, YM Choi, S Yoo, Y Ding, R Yan, K Pei, C Qu, L Zhang, I Chang, B Zhao, Y. Zhang, H. Chen, Yan Chen, C. Yang, B. deGlee, R. Murphy, J. Liu, M. Liu, "A Highly Efficient Multi-phase Catalyst Dramatically Enhances the Rate of Oxygen Reduction", ***Joule***, 2, 1-12 (2018)
3. Xiaxi Li, Kevin Blinn, Dongchang Chen, Meilin Liu, "In-situ and Surface Enhanced Raman Spectroscopy Study of Electrode Materials in Solid Oxide Fuel Cells", ***Electrochemical Energy Reviews***,1 (3), 433-459 (2018) | DOI: 10.1007/s41918-018-0017-9

4. H Xu, Y Chen, JH Kim, Z Dang, M Liu, "Lattice Boltzmann modelling of the coupling between charge transport and electrochemical reactions in a solid oxide fuel cell with a patterned anode" , ***International Journal of Hydrogen Energy*** 44 (57), 30293-30305 (2019).

References

[1] N. Q. Minh, "Ceramic Fuel-Cells," (in English), *J Am Ceram Soc,* vol. 76, no. 3, pp. 563-588, Mar 1993. [Online]. Available: <Go to ISI>://A1993LE27800001.

[2] B. C. H. Steele and A. Heinzel, "Materials for fuel-cell technologies," (in English), *Nature,* Article vol. 414, no. 6861, pp. 345-352, Nov 2001. [Online]. Available: <Go to ISI>://000172150700054

[3] S. C. Singhal, "Solid oxide fuel cells for stationary, mobile, and military applications," *Solid State Ionics,* vol. 152-153, pp. 405-410, 2002, doi: 10.1016/s0167-2738(02)00349-1.

[4] M. Liu, M. E. Lynch, K. Blinn, F. M. Alamgir, and Y. Choi, "Rational SOFC material design: new advances and tools," *Materials Today,* vol. 14, no. 11, pp. 534-546, Nov 2011. [Online]. Available: <Go to ISI>://WOS:000297256200017.

[5] L. Yang *et al.*, "Promotion of water-mediated carbon removal by nanostructured barium oxide/nickel interfaces in solid oxide fuel cells," (in eng), *Nat Commun,* Research Support, Non-U.S. Gov't Research Support, U.S. Gov't, Non-P.H.S. vol. 2, p. 357, 2011, doi: 10.1038/ncomms1359.

[6] L. Yang *et al.*, "Enhanced sulfur and coking tolerance of a mixed ion conductor for SOFCs: $BaZr_{0.1}Ce_{0.7}Y_{0.2-x}Yb_xO_{3-\delta}$ " (in eng), *Science,* Research Support, U.S. Gov't, Non-P.H.S. vol. 326, no. 5949, pp. 126-9, Oct 2 2009, doi: 10.1126/science.1174811.

[7] D. Ding, X. Li, S. Y. Lai, K. Gerdes, and M. Liu, "Enhancing SOFC cathode performance by surface modification through infiltration," *Energy & Environmental Science,* vol. 7, no. 2, pp. 552-575, 2014.

[8] H. Yokokawa, H. Y. Tu, B. Iwanschitz, and A. Mai, "Fundamental mechanisms limiting solid oxide fuel cell durability," *J Power Sources,* vol. 182, no. 2, pp. 400-412, Aug 2008, doi: 10.1016/j.jpowsour.2008.02.016.

[9] "SECA rewards Acumentrics progress in tubular SOFCs," *Fuel Cells Bulletin,* vol. 2004, no. 5, p. 1, 2004, doi: http://dx.doi.org/10.1016/S1464-2859(04)00157-9.

[10] J. A. Schuler, Z. Wuillemin, A. Hessler-Wyser, C. Comminges, N. Y. Steiner, and J. Van herle, "Cr-poisoning in (La,Sr)(Co,Fe)O3 cathodes after 10,000 h SOFC stack testing," *Journal of Power Sources,* vol. 211, no. 0, pp. 177-183, 8/1/ 2012, doi: http://dx.doi.org/10.1016/j.jpowsour.2012.03.045.

[11] J. A. Schuler *et al.*, "Combined Cr and S poisoning in solid oxide fuel cell cathodes," *J Power Sources,* vol. 201, pp. 112-120, Mar 2012, doi: 10.1016/j.jpowsour.2011.10.123.

[12] E. Konysheva *et al.*, "Chromium poisoning of perovskite cathodes by the ODS alloy Cr5Fe1Y(2)O(3) and the high chromium ferritic steel Crofer22APU," *J Electrochem Soc,* vol. 153, no. 4, pp. A765-A773, 2006, doi: 10.1149/1.2172563.

[13] S. P. Jiang, J. P. Zhang, and X. G. Zheng, "A comparative investigation of chromium deposition at air electrodes of solid oxide fuel cells," (in English), *J Eur Ceram Soc,* vol. 22, no. 3, pp. 361-373, Mar 2002. [Online]. Available: <Go to ISI>://000172935000013.

[14] S. P. Jiang, S. Zhang, and Y. D. Zhen, "Early interaction between Fe-Cr alloy metallic interconnect and Sr-doped LaMnO3 cathodes of solid oxide fuel cells," (in English), *J Mater Res,* vol. 20, no. 3, pp. 747-758, Mar 2005, doi: Doi 10.1557/Jmr.2005.0101.

[15] S. P. Jiang, Y. D. Zhen, and S. Zhang, "Interaction between Fe-Cr metallic interconnect and (La, Sr) MnO3/YSZ composite cathode of solid oxide fuel cells," (in English), *J Electrochem Soc,* vol. 153, no. 8, pp. A1511-A1517, 2006. [Online]. Available: <Go to ISI>://000238470100012.

[16] Y. D. Zhen, A. I. Y. Tok, F. Y. C. Boey, and S. P. Jiang, "Development of Cr-tolerant cathodes of solid oxide fuel cells," (in English), *Electrochem Solid St,* vol. 11, no. 3, pp. B42-B46, 2008, doi: Doi 10.1149/1.2828212.

[17] S. P. Jiang and Y. D. Zhen, "Mechanism of Cr deposition and its application in the development of Cr-tolerant cathodes of solid oxide fuel cells," (in English), *Solid State Ionics,* vol. 179, no. 27-32, pp. 1459-1464, Sep 30 2008, doi: DOI 10.1016/j.ssi.2008.01.006.

[18] T. Komatsu, H. Arai, R. Chiba, K. Nozawa, M. Arakawa, and K. Sato, "Cr poisoning suppression in solid oxide fuel cells using LaNi(Fe)O-3 electrodes," *Electrochem Solid St,* vol. 9, no. 1, pp. A9-A12, 2006, doi: 10.1149/1.2130309.

[19] M. K. Stodolny, B. A. Boukamp, D. H. A. Blank, and F. P. F. van Berkel, "La(Ni,Fe)O-3 Stability in the Presence of Chromia-A Solid-State Reactivity Study," *J Electrochem Soc,* vol. 158, no. 2, pp. B112-B116, 2011, doi: 10.1149/1.3519369.

[20] M. K. Stodolny, B. A. Boukamp, D. H. A. Blank, and F. P. F. van Berkel, "Impact of Cr-poisoning on the conductivity of LaNi0.6Fe0.4O3," *J Power Sources,* vol. 196, no. 22, pp. 9290-9298, Nov 2011, doi: 10.1016/j.jpowsour.2011.07.070.

[21] M. K. Stodolny, B. A. Boukamp, D. H. A. Blank, and F. P. F. van Berkel, "Cr-poisoning of a LaNi0.6Fe0.4O3 cathode under current load," *J Power Sources,* vol. 209, pp. 120-129, Jul 2012, doi: 10.1016/j.jpowsour.2012.02.083.

[22] Y. Chen *et al.*, "A robust and active hybrid catalyst for facile oxygen reduction in solid oxide fuel cells," *Energy & Environmental Science,* 10.1039/C6EE03656B vol. 10, no. 4, pp. 964-971, 2017, doi: 10.1039/C6EE03656B.

[23] M. Liu *et al.*, "Solid oxide fuel cells having porous cathodes infiltrated with oxygen-reducing catalysts," 2010.

[24] D. Ding *et al.*, "Efficient Electro-Catalysts for Enhancing Surface Activity and Stability of SOFC Cathodes," *Advanced Energy Materials,* vol. 3, no. 9, pp. 1149-1154, 2013, doi: 10.1002/aenm.201200984.

[25] M. E. Lynch *et al.*, "Enhancement of $La_{0.6}Sr_{0.4}Co_{0.2}Fe_{0.8}O_{3-\delta}$ durability and surface electrocatalytic activity by $La_{0.85}Sr_{0.15}MnO_{3\pm\delta}$ investigated using a new test electrode platform," *Energy & Environmental Science,* vol. 4, no. 6, p. 2249, 2011, doi: 10.1039/c1ee01188j.

[26] X. Y. Lou, S. Z. Wang, Z. Liu, L. Yang, and M. L. Liu, "Improving La0.6Sr0.4Co0.2Fe0.8O3-δ cathode performance by infiltration of a Sm0.5Sr0.5CoO3-δ coating," (in English), *Solid State Ionics,* vol. 180, no. 23-25, pp. 1285-1289, Oct 5 2009, doi: DOI 10.1016/j.ssi.2009.06.014.

[27] M. Liu, D. Ding, K. Blinn, X. Li, L. Nie, and M. Liu, "Enhanced performance of LSCF cathode through surface modification," *International Journal of Hydrogen Energy,* 2012, doi: 10.1016/j.ijhydene.2012.02.139.

[28] L. F. Nie, M. F. Liu, Y. J. Zhang, and M. L. Liu, "La0.6Sr0.4Co0.2Fe0.8O3-δ cathodes infiltrated with samarium-doped cerium oxide for solid oxide fuel cells," (in English), *J Power Sources,* vol. 195, no. 15, pp. 4704-4708, Aug 1 2010, doi: DOI 10.1016/j.jpowsour.2010.02.049.

[29] B. Rivas-Murias and V. Salgueiriño, "Thermodynamic CoO–Co3O4 crossover using Raman spectroscopy in magnetic octahedron-shaped nanocrystals," *Journal of Raman Spectroscopy,* vol. 48, no. 6, pp. 837-841, 2017.

[30] A. Glamazda *et al.*, "Structural instability of the CoO4 tetrahedral chain in SrCoO3− δ thin films," *Journal of Applied Physics,* vol. 118, no. 8, p. 085313, 2015.

[31] M. Zhang, M. de Respinis, and H. Frei, "Time-resolved observations of water oxidation intermediates on a cobalt oxide nanoparticle catalyst," *Nature Chemistry,* Article vol. 6, p. 362, 02/23/online 2014, doi: 10.1038/nchem.1874 https://www.nature.com/articles/nchem.1874#supplementary-information.

[32] M.-h. Shao, P. Liu, and R. R. Adzic, "Superoxide anion is the intermediate in the oxygen reduction reaction on platinum electrodes," *Journal of the American Chemical Society,* vol. 128, no. 23, pp. 7408-7409, 2006.

[33] H.-Y. Wang *et al.*, "In Situ Spectroscopic Identification of μ-OO Bridging on Spinel Co3O4 Water Oxidation Electrocatalyst," *The Journal of Physical Chemistry Letters,* vol. 7, no. 23, pp. 4847-4853, 2016/12/01 2016, doi: 10.1021/acs.jpclett.6b02147.

[34] Z. Wang, R. Peng, W. Zhang, X. Wu, C. Xia, and Y. Lu, "Oxygen reduction and transport on the La1-xSrxCo1-yFeyO3-[small delta] cathode in solid oxide fuel cells: a first-principles study," *Journal of Materials Chemistry A,* 10.1039/C3TA11554B vol. 1, no. 41, pp. 12932-12940, 2013, doi: 10.1039/C3TA11554B.

[35] Y. Choi, M. e. C. Lin, and M. Liu, "Computational study on the catalytic mechanism of oxygen reduction on La0. 5Sr0. 5MnO3 in solid oxide fuel cells," *Angewandte Chemie International Edition,* vol. 46, no. 38, pp. 7214-7219, 2007.

[36] Y. Chen *et al.*, "A Highly Efficient Multi-phase Catalyst Dramatically Enhances the Rate of Oxygen Reduction," *Joule,* 2018.